Vacuum 245 (2026) 114812

Contents lists available at ScienceDirect

Vacuum

journal homepage: www.elsevier.com/locate/vacuum

Nickel oxide hole transport layer for perovskite solar cells: Preparation via pulsed laser deposition with simulation and experimental insights

Eva Horynova [a,*], Jakub Holovsky [a,b], Lucie Landova [a,b], Naini Jain [a], Abhinav Deep Pakki [a], Meng-Hsueh Kuo [a,b], Ivana Beshajová Pelikánová [a], Branislav Dzurňák [a], Lukáš Horák [c], Ognen Pop-Georgievski [d], Amalraj Peter Amalathas [a,e], Neda Neykova [a,b]

[a] Centre for Advanced Photovoltaics, Faculty of Electrical Engineering, CTU in Prague, Technická 2, 166 27, Prague, Czech Republic
[b] Institute of Physics, Czech Academy of Sciences, Cukrovarnická 10, 162 00, Prague, Czech Republic
[c] Department of Condensed Matter Physics, Faculty of Mathematics and Physics, Charles University, Ke Karlovu 2026/5, Praha 2, Prague, 121 16, Czech Republic
[d] Institute of Macromolecular Chemistry, Czech Academy of Sciences, Heyrovskeho nam. 2, 162 00, Prague, Czech Republic
[e] Department of Physics, Faculty of Science, University of Jaffna, Jaffna, 40000, Sri Lanka

ARTICLE INFO

Keywords:
Pulsed laser deposition
Nickel oxide
Perovskite solar cells
Hole transport layer

ABSTRACT

Nickel oxide (NiO_x) has gained attention as a promising inorganic hole transport layer for perovskite solar cells due to its wide bandgap, high transparency, and stability. However, tuning of band alignment by an extra dipole layer is necessary to achieve high efficiencies. Our predictive simulations suggest that NiO_x bandgap tuning can also improve solar cell performance. Motivated by these findings, this study experimentally investigates NiO_x films with different bandgap fabricated using pulsed laser deposition under varying deposition conditions, including oxygen pressure, substrate temperature and laser frequency. Our outcomes show that mainly the deposition temperature significantly influences the chemical composition, optical properties, and defect states in the NiO_x films, lattice constants and morphology as confirmed by X-ray photoelectron spectroscopy, photothermal deflection spectroscopy, X-ray diffraction spectroscopy, atomic force microscopy and scanning electron microscopy. Experimentally, $FA_{0.83}Cs_{0.17}Pb(I_{0.6}Br_{0.4})_3$ mixed halide perovskite solar cells were fabricated on NiO_x substrates prepared under varying oxygen pressures and pulse numbers, achieving a maximum power conversion efficiency of approximately 8 %. This demonstrates that NiO_x deposited by pulsed laser deposition, when properly tuned, is a promising candidate for an efficient hole transport layer in perovskite-based photovoltaics.

1. Introduction

Perovskite solar cells (PSCs) have emerged as a revolutionary photovoltaic technology due to their remarkable power conversion efficiencies (PCEs) and relatively simple fabrication processes [1–3]. The laboratory scale PCEs have boosted from 3.5 % [4] to 26.7 % [5] since PSCs inception in 2009. Among the various materials used in PSCs, mixed-halide perovskites offer the advantage of tunable optoelectronic properties, making them suitable for highly efficient PSCs [6]. However, the performance of these solar cells is strongly influenced by the quality and optimisation of charge transport layers [7]. The operational efficiency of PSCs relies heavily on the effective separation and transport of photogenerated charge carriers—electrons and holes—from the perovskite absorber to their respective electrodes. To achieve this, two critical components are incorporated: the electron transport layer (ETL) and the hole transport layer (HTL). While the ETL facilitates the movement of electrons and blocks holes, the HTL performs the opposite role, allowing the selective transport of holes while blocking electron backflow. Together, these transport layers enable efficient charge separation and reduce recombination losses, which are essential for high-performance solar cells [8]. The impact of both ETLs and HTLs is crucial. However, the HTL plays a crucial role in extracting photo-generated holes while maintaining high transparency [9,10]. Additionally, compared to ETLs, HTLs often face greater challenges in balancing conductivity, chemical

This article is part of a special issue entitled: EVC-17/ECOSS-37 published in Vacuum.

* Corresponding author.
E-mail address: eva.horynova@fel.cvut.cz (E. Horynova).

https://doi.org/10.1016/j.vacuum.2025.114812
Received 30 September 2024; Received in revised form 1 October 2025; Accepted 7 October 2025
Available online 10 November 2025

stability, and compatibility with perovskite layers, especially under ambient conditions where degradation can occur.

Thus, the choice of materials for the HTL is essential for the overall stability and cost-effectiveness of PSCs. Effective organic HTLs like 2,2′,7,7′-Tetrakis[N,N-di(4-methoxyphenyl)amino]-9,9′-spiro-bifluorene (Spiro-MeOTAD), Poly(3,4-ethylenedioxythiophene) (PEDOT), and Poly[bis(4-phenyl)(2,4,6-trimethylphenyl)amine] (PTAA) tend to be more expensive and less stable. This makes inorganic alternatives a more attractive option for enhancing the longevity and affordability of PSCs [3]. Transition metal oxides, such as NiO_x CuO_x, MoO_3, Cr_2O_3, WO_3, and V_2O_5, have been widely used as HTLs because they are intrinsically stable under environmental impacts and offer low cost and relatively easy fabrication since they can be deposited via solution process. NiO_x is a p-type semiconductor material that has been increasingly utilised as a HTL in PSCs due to its wide bandgap (typically 3.6–4.0 eV), high transparency, and suitable energy-level alignment with perovskites [11]. NiO_x offers improved stability compared to organic HTLs like Spiro-OMeTAD, and its performance can be tailored by modifying its physical properties during deposition. When compared to other metal oxides, NiO_x offers a superior combination of stability, hole mobility, energy band alignment, transparency, and cost-effectiveness, making it an ideal HTL material for perovskite solar cells. Moreover, NiO_x has minimal reactivity with perovskite layers, reducing the risk of interfacial degradation or unwanted reactions that can occur with other metal oxides, like MoO_3. Recently, inverted PSCs with NiO_x have been reported as HTL, with a certificated efficiency of 26.08 % and excellent long-term stability [12]. Several techniques can be used to deposit NiO_x layers, including spin coating [13,14], thermal evaporation [13], and different types of sputtering [15–17]. However, pulsed laser deposition (PLD) offers numerous advantages over these techniques in terms of controlling film thickness, composition, and other properties through adjustments in deposition parameters such as substrate temperature, oxygen pressure, and laser fluence [18]. These parameters can have a significant impact on the resulting band gap of the NiO_x films, which, in turn, influences the performance of PSCs [19].

In this study, we focus on the preparation of NiO_x thin films as HTLs in PSCs using PLD, investigating their properties through both simulation studies and experimental methods. The choice of NiO_x as an HTL, along with insights gained from simulation, aims to advance the understanding of hole transport in PSCs, thereby contributing to the development of more stable and efficient devices. Although this study does not focus on optimisation, it seeks to confirm the trends observed in the simulation by preparing NiO_x films via PLD under different oxygen pressures, substrate temperatures, and laser frequencies. The experimental results will provide insights into how PLD parameters influence NiO_x properties and their application as HTLs in PSCs. The prepared films are characterised by photothermal deflection spectroscopy (PDS), X-ray photoelectron spectroscopy (XPS), X-ray diffraction spectroscopy (XRD), Atomic force microscopy (AFM) and Scanning electron microscopy (SEM) followed by the fabrication and J-V measurement of PSC devices incorporating NiO_x as HTL. To determine the optimal conditions for fabricating NiO_x films for use as HTLs in PSCs, we analysed the effects of temperature, laser frequency, and oxygen pressure during PLD.

2. Experimental methods

2.1. Numerical simulations

To provide further motivation for investigating NiO_x films deposited under different PLD conditions, a one-dimensional (1D) simulation of a $FA_{0.83}Cs_{0.17}Pb(I_{0.6}Br_{0.4})_3$ mixed halide PSCs with a NiO_x as HTL was conducted. The simulation uses the Silvaco TCAD device simulator to model the performance of p-i-n perovskite solar cells, focusing on optimising NiO_x parameters. The simulated device structure consists of an ITO/NiO_x/Perovskite/PCBM/BCP/Ag stack on a 400 nm thick $FA_{0.83}Cs_{0.17}Pb_3(I_{0.6}Br_{0.4})_3$ perovskite absorber, doped at 10^{14} cm^{-3}, where ITO is indium thin oxide, PCBM is metanofullerene Phenyl-C61-Butyric-Acid-Methyl-Ester, BCP is Bathocuproine and Ag is silver. The front and rear contact consists of ITO/NiO_x and BCP/Ag interfaces, with work functions of approximately 5.1 eV and 4.0 eV. The objective of the simulation study is to examine the impact of NiO_x layer thickness, ranging from 10 to 100 nm, and energy band gap variations from 3.2 to 4.0 eV, on the performance of PSCs. For this study, a one-dimensional (1D) simulation was executed, incorporating updated models to enhance accuracy. This simulation is also simplified based on the assumption of solely planar contacts and the negligible contribution of the lateral path to current flow. The photovoltaic parameters were extracted. A table with the electrical parameters for the various layers in the simulation of PSCs is presented in Supporting information (Table S1).

The simulation investigated the influence of NiO_x band gap and film thickness on photovoltaic parameters of PSCs, such as fill factor (FF), open-circuit voltage (V_{OC}), short-circuit current density (J_{SC}) and power conversion efficiency (PCE).

Table 1
Different settings of the pulse laser depositions of NiO_x used for the evaluation of the effect of temperature, repetition rate and oxygen pressure.

	effect of temperature	effect of laser frequency	effect of oxygen pressure
temperature (°C)	**25–400**	25	25
oxygen pressure (mbar)	0.1	0.1	**0.08–0.12**
laser frequency (Hz)	50	**5–50**	50

2.2. Experimental study

2.2.1. NiO_x layer deposition by PLD

In the initial phase of the experiment, we applied samples onto 10 × 10 mm^2 glass, fused silica, and silicon substrates to prepare suitable specimens for PDS, ellipsometry, XPS, XRD, AFM and SEM measurements. The deposition process involved PLD in a chamber evacuated to 1 × 10^{-5} mbar, followed by introducing varying oxygen levels ranging from 0.08 to 0.12 mbar while maintaining a continuous oxygen flow of 10 sccm. The samples were positioned in a heated holder rotating at 5 rpm and then heated to different temperatures from room temperature to 400 °C. The target composition was NiO, and it was rotating at 28.9 rpm and ablated using a KrF excimer laser COMPex 50 with repetition rates ranging from 5 Hz to 50 Hz and laser energy set to 125 mJ. Each sample received 15,000 pulses, resulting in 40–60 nm thicknesses. All the different settings used in the first part of the experiment can be seen in Table 1.

The samples were evaluated using a combination of PDS and ellipsometry, enabling observation of optical spectra ranging from 1.5 to 6.5 eV. PDS was conducted in isopropanol with a refractive index of 1.38.

After the measurements and simulations, the most promising deposition combinations were identified, and samples with these parameters were prepared. PLD was applied on 20 × 20 mm^2 glass substrates with a pre-existing patterned ITO layer (14 × 20 mm^2). The chamber was evacuated to 1 × 10^{-5} mbar, after which oxygen was introduced at a range of 0.08–0.25 mbar. The substrates were then heated to 25 °C, 200 °C, and 400 °C to explore a wide temperature range, as these settings appeared suitable based on bandgap evaluations. However, it was found that at higher temperatures, the perovskite material failed to adhere to the surface, making it impossible to prepare perovskite solar cells on these samples. Consequently, for the fabrication of the solar cells, NiO_x layers prepared at room temperature were used.

When considering the repetition rate of the laser, it is important to note that higher frequencies lead to greater sub-band gap absorption, as seen in Fig. 4. Because of this, a frequency of 5 Hz was ultimately chosen

Table 2
Different settings of the pulse laser depositions of NiO_x further used as hole transport layer in solar cell devices.

	effect of temperature	effect of oxygen pressure	effect of thickness
temperature (°C)	**25–400**	25	25
oxygen pressure (mbar)	0.1	**0.08–0.25**	0,1
number of pulses	2000	2000	**1000–8000**

for all the samples.

Thickness was also a tested parameter, so the number of pulses differed from 1000 to 8000, resulting in roughly 8–50 nm thick samples. All of the settings used in the first part of the experiment can be seen in Table 2.

2.2.2. *Fabrication of $FA_{0.83}Cs_{0.17}Pb(I_{0.6}Br_{0.4})_3$ mixed halide p-i-n perovskite solar cell*

Patterned ITO substrates were subsequently cleaned in the solvents of deionised water, ethanol, acetone, and isopropyl alcohol. Then, the hole-transport material NiO_x was deposited by PLD at different conditions. The perovskite films with the following chemical composition $FA_{0.83}Cs_{0.17}Pb(I_{0.6}Br_{0.4})_3$ were deposited on the NiO_x layer. A detailed description of the perovskite fabrication process can be found elsewhere [20]. Subsequently, the electron transport material [6,6]-phenyl-C 61 -butyric acid methyl ester ($PC_{61}BM$, 20 mg/ml in anhydrous chlorobenzene) was deposited on perovskite films by spin coating at 2000 rpm for 30 s, followed by spin-coating of buffer layer (bathocuproine, BCP) with the concentration of 0.5 mg/ml in 2-propanol on top (4000 rpm, 30 s). Finally, silver electrodes with a thickness of 120 nm were deposited by thermal evaporation.

For details about PDS, ellipsometry, XPS, XRD, SEM, AFM and J-V measurement, refer to Supplementary Information.

3. Results and discussion

The simulation results, presented in Fig. 1, demonstrate that increasing the bandgap of the NiO_x layer from 3.2 eV to 4.0 eV leads to substantial improvements in both fill factor and efficiency. This suggests that wider bandgap NiO_x layers can enhance charge extraction and minimise recombination losses at the interface with the perovskite absorber. In contrast, the effect of NiO_x thickness on solar cell performance appears minimal, with negligible variations in V_{OC} and a slight increase in J_{SC} as the thickness changes from 10 nm to 100 nm.

These simulation findings motivate the need to experimentally investigate NiO_x films with varying deposition conditions to evaluate

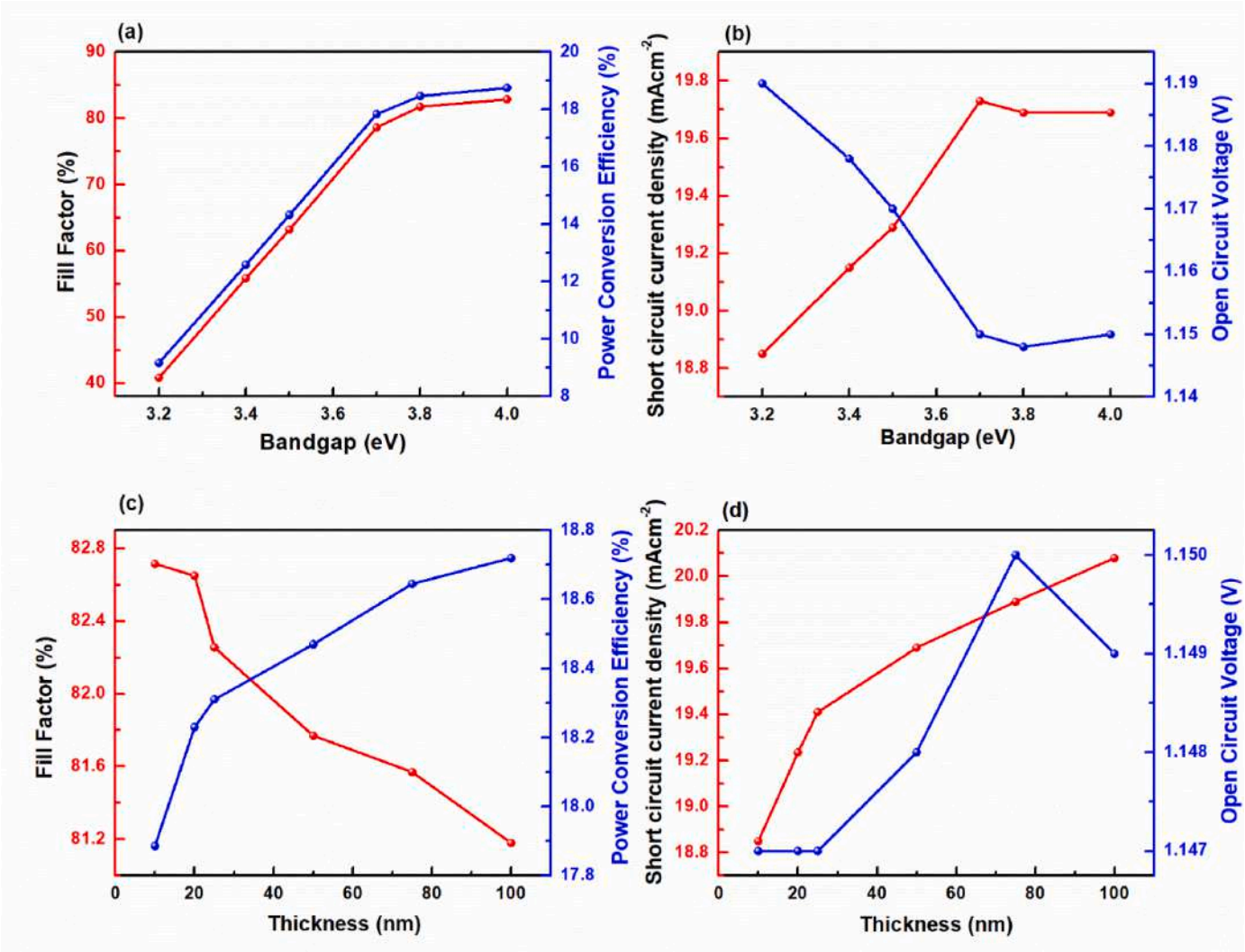

Fig. 1. Simulated effect of NiO_x bandgap on (a) Fill Factor and Power Conversion Efficiency and (b) Short Circuit Current Density and Open Circuit Voltage in a perovskite solar cell and simulated effect of NiO_x layer thickness (c) Fill Factor and Power Conversion Efficiency and (d) Short Circuit Current Density and Open Circuit Voltage in a perovskite solar cell.

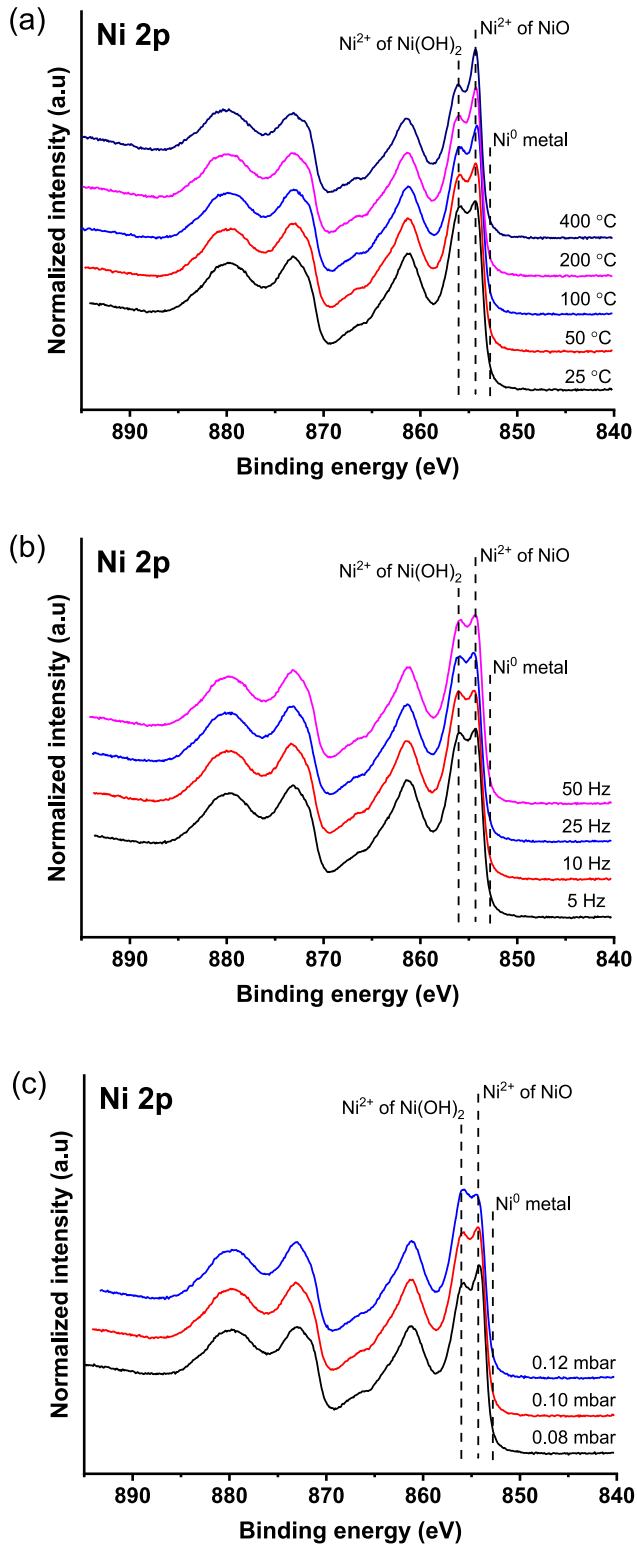

Fig. 2. Evolution of high-resolution XPS spectra taken in the Ni 2p region for NiO PDL films deposited at varying (a) temperature, (b) laser frequency and (c) oxygen pressure (at a representative laser frequency of 50 Hz). Eye guidelines are given at metal Ni, NiO and $Ni(OH)_2$ contributions.

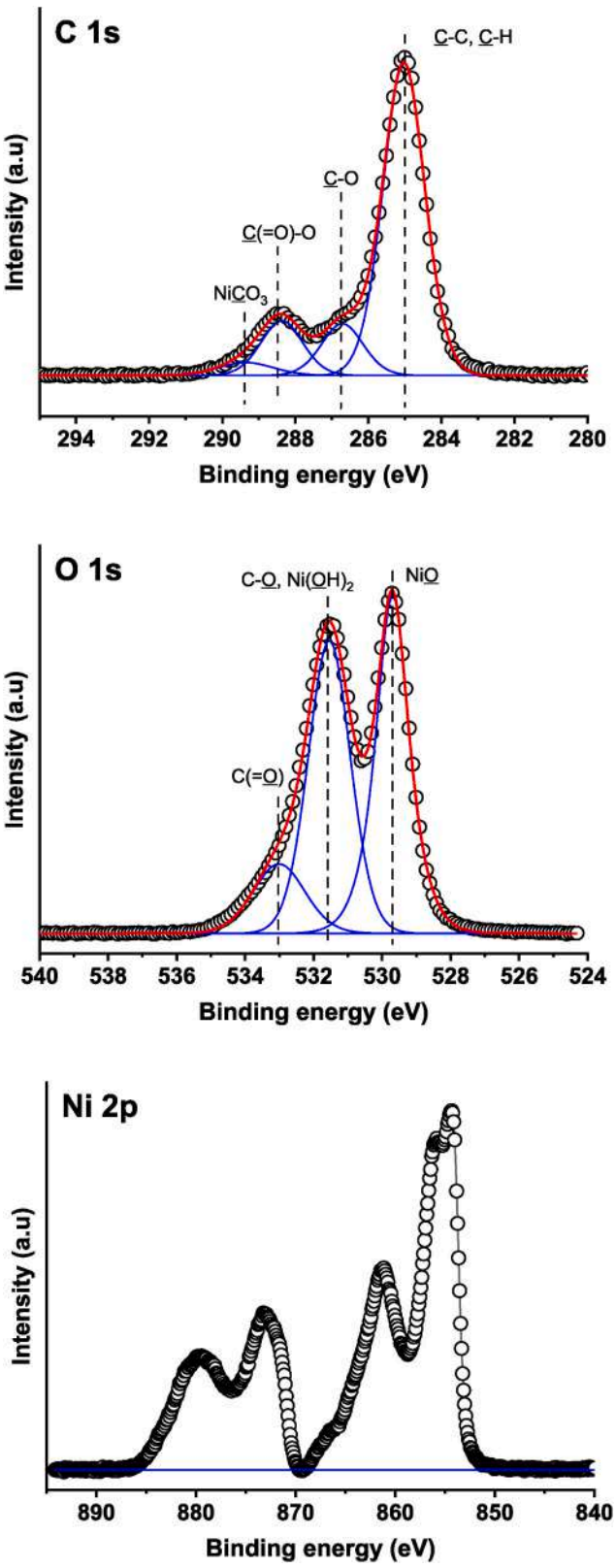

Fig. 3. Representative high-resolution XPS spectra of NiO PLD film (deposited at 25 °C, oxygen pressure of 0.1 mbar, and laser frequency of 50 Hz) in C 1s, O 1s, and Ni 2p regions. Measured spectra are shown in open circles, whereas their fittings are shown in red lines. The individual contributions of different functional groups are displayed in blue lines.

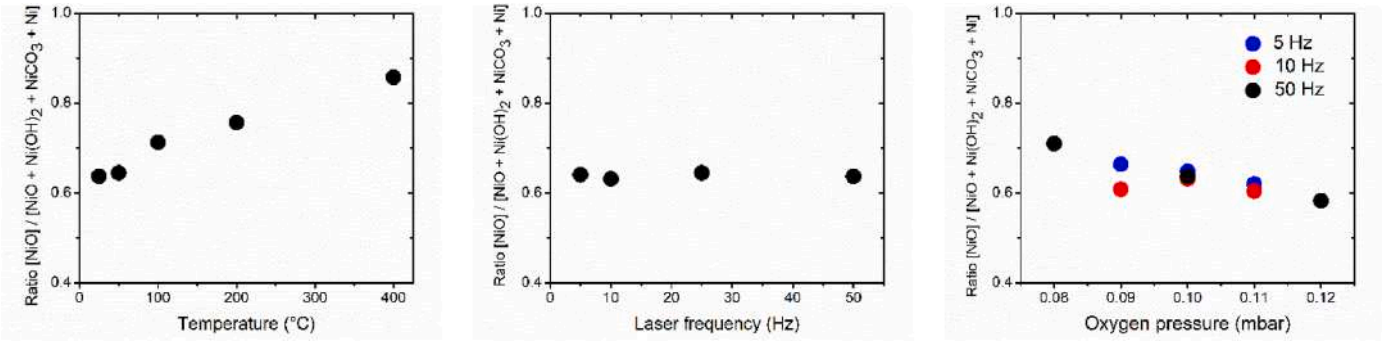

Fig. 4. Ratio between the amount of NiO and other nickel oxygen species ($Ni(OH)_2$ and $NiCO_3$) under varying pulsed laser deposition conditions (a) temperature, (b) laser frequency and (c) oxygen pressure, as determined via XPS analysis.

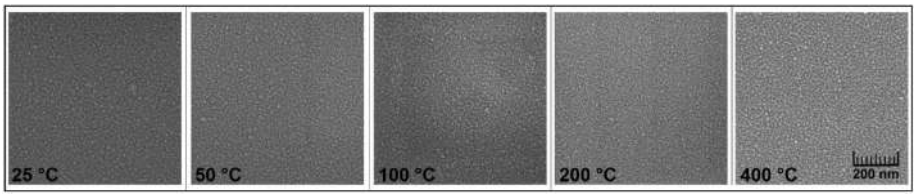

Fig. 5. SEM images of NiO_x layers deposited at a constant pressure of 0.1 mbar, constant frequency of 50Hz and different temperatures of 25, 50, 100, 200 and 400 °C, respectively.

their band gap and subsequent impact on solar cell efficiency. In the first step of our experimental study, we determined the chemical composition and the oxidation state of Ni of the NiO_x films using XPS analysis.

Evolution of high-resolution XPS spectra taken in the Ni 2p region for NiO PDL films deposited at varying temperature, laser frequency and oxygen pressure (at a representative laser frequency of 50 Hz) in shown in Fig. 2. Eye guidelines are given at metal Ni, NiO and $Ni(OH)_2$ contributions.

In Fig. 3 are shown representative high-resolution XPS spectra of NiO PLD film (deposited at 25 °C, oxygen pressure of 0.1 mbar, and laser frequency of 50 Hz) in C 1s, O 1s, and Ni 2p regions. Measured spectra are shown in open circles, whereas their fittings are shown in red lines. The individual contributions of different functional groups are displayed in blue lines.

Based on the chemical composition (Figs. 2 and 3), we calculated the ratio between NiO and other Ni-oxygen species present on the surface of NiO_x films. The $[NiO]/[Ni + NiO + Ni(OH)_2 + NiCO_3]$ amount ratio can be utilised as a guideline for the dominance of NiO within the thin film structure (Table S2). Fig. 4 shows the variation of the ratio $[NiO]/[Ni + NiO + Ni(OH)_2 + NiCO_3]$ as a function of deposition temperature, laser frequency, and oxygen pressure during PLD. The ratio $[NiO]/[Ni + NiO + Ni(OH)_2 + NiCO_3]$ increases from about 0.6 to about 0.9 with respective increasing temperatures from room T to 400 °C. At the same time, the variation of laser frequency at constant temperature and oxygen pressure does not seem to have a decisive influence on the determined ratio. However, as the oxygen pressure increases from 0.08 mbar to 0.12 mbar, the ratio $[NiO]/[Ni + NiO + Ni(OH)_2 + NiCO_3]$ gradually decreases from about 0.7 to 0.6, respectively, with a seemingly limited effect of the oxygen pressure and laser frequency as previously noted. These findings indicate that we can systematically vary the amount of NiO and other Ni-species, such as $Ni(OH)_2$ and $NiCO_3$, through precise tuning of the PLD processing conditions.

Scanning electron microscopy was applied to analyse the morphology of the NiO_x layers. The SEM images presented in Fig. 5 show that continuous and conformal NiO_x layers are deposited. SEM data show that the films have a uniform surface morphology that exhibits round features, the diameter of which does not change as a function of deposition conditions. The NiO_x deposited at high frequency (50Hz) and high pressure (0.12 mbar) exhibits some nanocracks of the layer observed (Fig. 7). However, no noticeable difference in the diameter of the nanocolumns is observed compared to the layer deposited at lower frequencies.

The surface roughness of deposited NiO_x layers was determined by AFM. Fig. 8 shows AFM scans of the NiO_x layers deposited at different temperatures from 25 to 400 °C. The RMS roughness of the layers increases almost linearly with increasing the deposition temperature from 5.2 ± 0.1 nm at 25 °C to 12 ± 1.6 nm at 400 °C. This is in good agreement with SEM results.

In Fig. 9 are presented the measured X-ray diffraction patterns of the NiO_x films deposited by PLD at different conditions (frequency, pressure and temperature, respectively) showing clearly the polycrystalline nature of the films.

Fig. 10 shows the fitted XRD patterns of NiO_x films deposited at a constant pressure of 0.1 mbar, constant frequency of 50 Hz, and varying

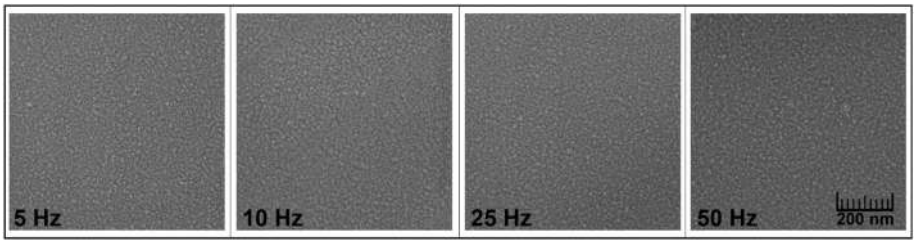

Fig. 6. SEM images of NiO_x layer deposited at constant T of 25 °C, constant pressure of 0.1 mbar and different frequencies: 5, 10, 25 and 50Hz.

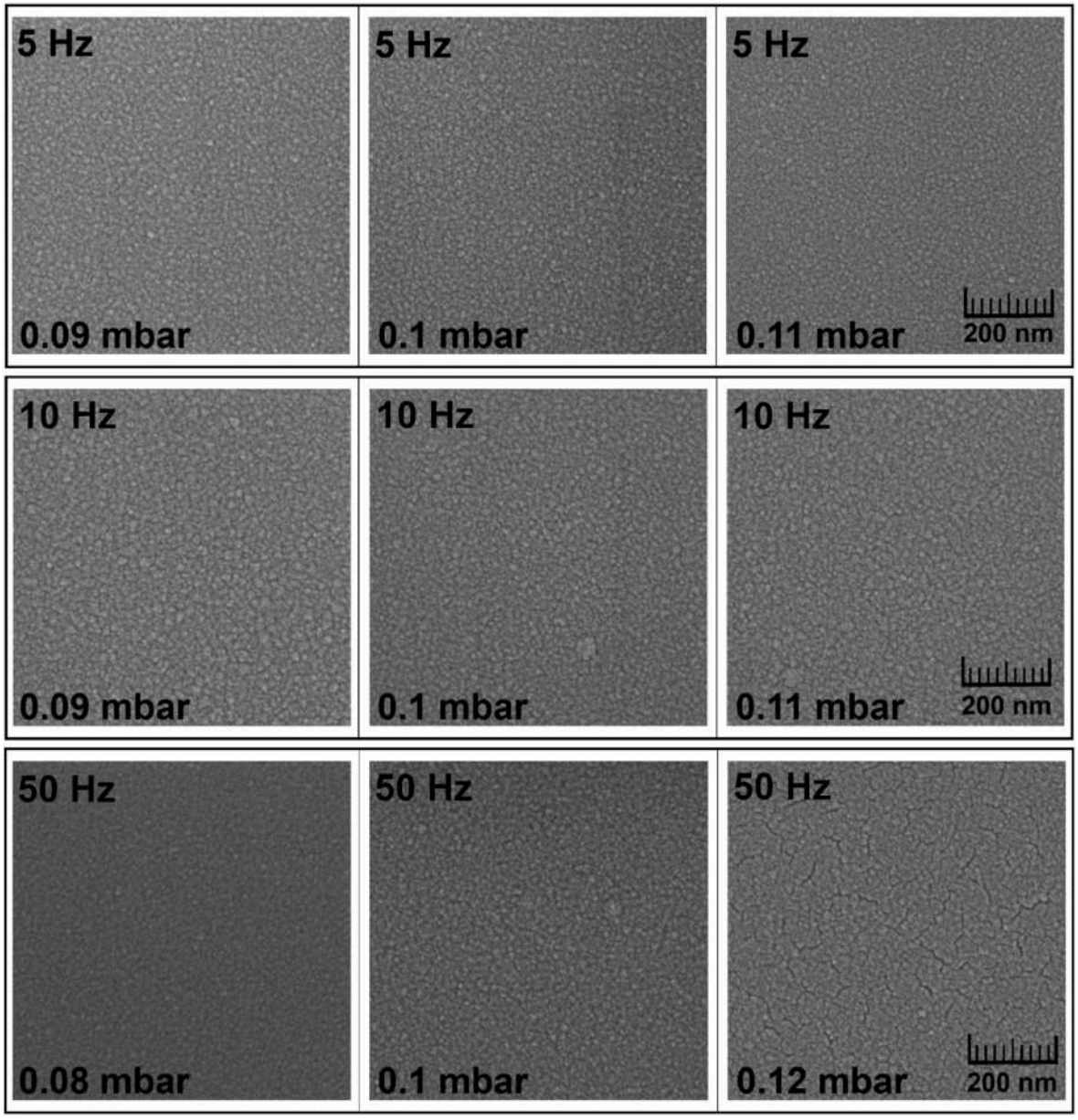

Fig. 7. SEM images of NiO_x layer deposited at constant T of 25 °C, different frequency (5Hz, 10Hz and 50Hz) and different pressures.

temperatures. All deposited films primarily consist of the NiO cubic phase, with a minor trace of metallic Ni. Rietveld analysis of the XRD patterns, measured at a fixed small incidence angle, was used to determine the cubic lattice parameter, residual stress in the films, mean crystallite size, and microstrain. A summary of these microstructural parameters is provided in Table 3 and visualized on the right side of Fig. 6.

The peak broadening analysis reveals that microstrain decreases and mean crystallite size increases with higher deposition temperatures. From the shifts in peak positions, it follows that all films exhibit tensile residual stress, which shows no significant dependence on deposition temperature. The refined lattice parameter systematically decreases with increasing deposition temperature, while remaining above the value for stoichiometric bulk NiO. The lattice parameter is influenced not only by stoichiometry but also by defect density (microstrain) and crystallite size. According to the XPS analysis (Table S2), there is a slight oxygen deficiency in NiO that increases with deposition temperature, which can affect the lattice parameter. At the same time, the release of microstrain and the increase in crystallite size at higher deposition temperatures contribute to the decrease in the lattice parameter towards the bulk value. These results are consistent with the findings of Fiévet et al. [21], who reported that the lattice parameter decreases with increasing crystallite size, decreasing microstrain, and the reduction of non-stoichiometric excess oxygen. Understandably, the XRD and XPS analysis point to different amounts of metallic Ni (but still in the same order of magnitude, i.e. not exceeding 3 % for both techniques, Table 3 and Table S2). The slight discrepancies mainly stem from the fact that while the XRD measurements are sensitive to the bulk material, the XPS is limited to the most outer 7–12 nm. We have to note that to a certain extent the presented XPS analysis suffers from the indirect determination of the individual Ni, NiO, $Ni(OH)_2$, and $NiCO_3$ contributions, mainly stemming from the complexity of the spectra.

The optical bandgap of NiO_x thin films was calculated using the absorption coefficient using the Tauc plot method where $(\alpha h\nu)^2$ was plotted over $h\nu$. Fig. 11 shows the bandgap variation as a function of deposition temperature, laser frequency, and oxygen pressure during PLD. The bandgap showed only a weak dependence on temperature, decreasing slightly from 3.65 eV at 100 °C to 3.5 eV at 400 °C. (see

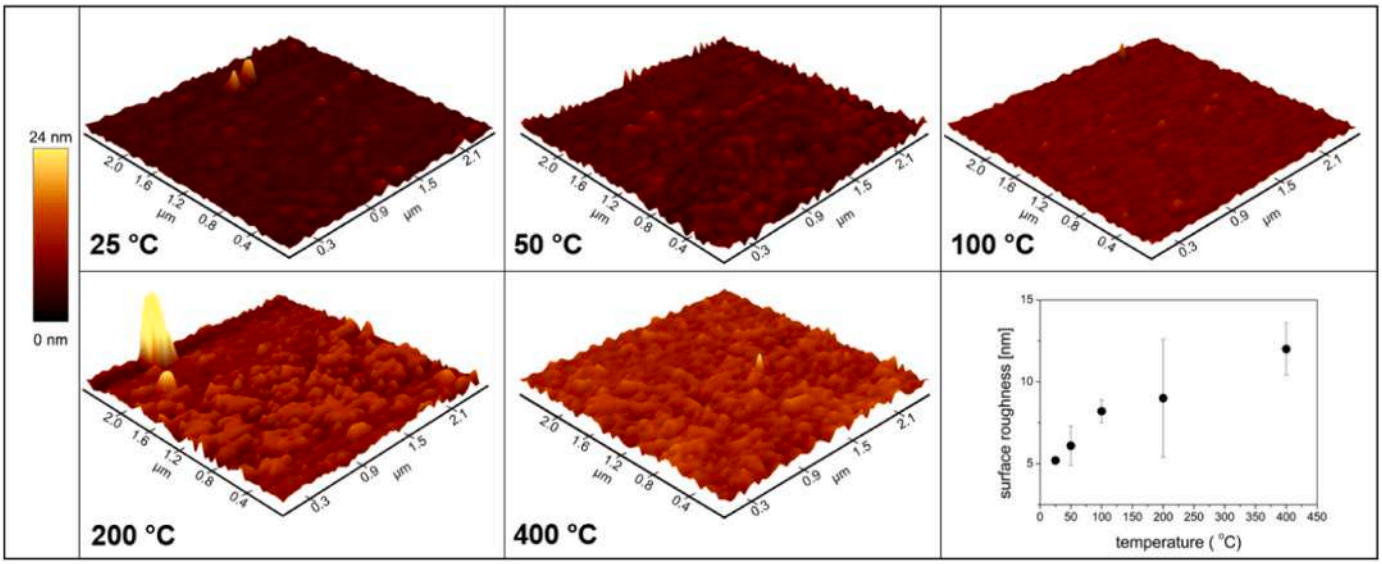

Fig. 8. AFM scans of NiO_x layers deposited at a constant pressure of 0.1 mbar and constant frequency of 50Hz and different temperatures of 25, 50, 100, 200 and 400 °C, as well as surface roughness-temperature dependence.

Fig. 11(a)). As shown in Fig. 11(b), the bandgap is around 3.8 eV at 5 Hz and slightly decreases at 25 Hz. However, a more significant drop occurs at 50 Hz, where the bandgap decreases to approximately 3.6 eV. This notable shift at higher frequencies suggests that increasing the laser frequency introduces more defects or reduces film quality, which negatively impacts the electronic properties of the NiO_x layer. Interestingly, on the surface, we determined that the stoichiometric coefficient in the NiO_x films was in the range of 0.92–1.03 (See Table S2), close to the expected stoichiometric coefficient of nickel (II) oxide x = 1.0. A clear trend is observed with increasing temperature and a drop of the determined stoichiometric coefficient from $NiO_{0.96}$ to $NiO_{0.92}$. Nevertheless, in all studied cases, we did not observe a rise in the stoichiometric coefficient to values of 1.5, indicative of the formation of Ni^{3+} species of Ni_2O_3 or NiOOH, as suggested by other authors [21]. Notably, the main spectral contributions/peaks appear at 852.8 eV, 854.3 eV and 856.1 eV originating from nickel species of Ni metal, NiO and $Ni(OH)_2$, respectively (See Figs. 2 and 3). These fall well apart from the expected Ni^{3+} of Ni_2O_3 or NiOOH, which should appear at 858.1 eV as proposed in the thorough work by Grosvenor et al. As the oxygen pressure increases from 0.08 mbar to 0.12 mbar, the bandgap gradually increases, reaching up to 3.8 eV at 0.12 mbar. At higher oxygen pressures, it is likely that the bulk structure of the film is better oxygenated and more stoichiometric, leading to reduced oxygen vacancies and a wider bandgap [22]. However, the surface composition (as probed by XPS) may show an increasing amount of hydroxides and carbonates, as surface reactions with environmental moisture or CO_2 can lead to the formation of these species. Essentially, while the surface becomes enriched in non-stoichiometric species (such as $Ni(OH)_x$ and $NiCO_x$), the bulk of the film maintain a high predominance of stoichiometric NiO species and Ni metal (as proven by XRD), explaining the bandgap widening.

Fig. 12 shows the absorption measured using a combination of PDS and ellipsometry for NiO_x films deposited under varying PLD conditions such as deposition temperature, laser frequency, and oxygen pressure.

Sub-bandgap absorption increases with rising temperature, especially beyond 100 °C. At 400 °C, the absorption is significantly higher compared to lower temperatures. The increase in sub-bandgap absorption at higher temperatures correlates with the formation of defect states, such as oxygen vacancies or grain boundaries, which introduce mid-gap states that allow sub-bandgap photons to be absorbed [23]. This suggests that higher temperatures lead to poor film quality with more defects, which can be detrimental to the performance of NiO_x as a hole transport layer in PSCs. The sub-bandgap absorption is lowest at 5 Hz and 25 Hz, but increases sharply at 50 Hz, indicating more defect-related absorption at this higher frequency. The sharp rise in sub-bandgap absorption at 50 Hz further supports the idea that higher laser frequencies cause greater defect formation. These defects increase the number of mid-gap states, leading to higher sub-bandgap absorption, which implies more recombination centres and lower film quality. With increasing oxygen pressure, sub-bandgap absorption decreases, showing lower absorption levels at 0.12 mbar compared to 0.08 mbar. The decrease in sub-bandgap absorption with increasing oxygen pressure indicates that higher oxygen pressures reduce the number of defect states in the NiO_x films. With fewer oxygen vacancies and other structural defects, there are fewer energy states within the bandgap. This reduction in defect states leads to decreased sub-bandgap absorption, which can improve film quality and reduce non-radiative recombination.

In the second step, based on the observations from both bandgap and sub-bandgap absorption analysis, we selected deposition conditions for the fabrication of NiO_x as a hole transport layer in perovskite solar cells. Specifically, we chose a low laser frequency of 5 Hz and a low deposition temperature of room temperature (25 °C) while varying the oxygen pressure between 0.08 mbar and 0.25 mbar. Given our earlier observations of increased bandgap and reduced sub-bandgap absorption at higher oxygen pressures, we selected these conditions for further study. Choosing a low frequency (5 Hz) and room temperature minimises the introduction of additional defects that may arise at higher frequencies and temperatures, as seen in the above results. These conditions help maintain the balance between controlling the bandgap and minimising the formation of sub-bandgap defects, which is important for achieving efficient charge extraction and transport in perovskite solar cells. The decision to vary oxygen pressure is particularly important since higher oxygen pressures have been shown to suppress sub-bandgap defect formation by reducing oxygen vacancies, which are a common source of recombination losses in solar cell devices.

The J-V measurements conducted with varying oxygen pressures yielded insightful results regarding the efficiency of the mixed halide $FA_{0.83}Cs_{0.17}Pb(I_{0.6}Br_{0.4})_3$ perovskite solar cells using NiO_x as the hole transport layer. The box plots in Fig. 13(a) show a wide distribution in efficiency values, indicating some variability in device performance as a function of oxygen pressure during the pulsed laser deposition process. At low oxygen pressures of 0.08 mbar, the average efficiency remained notably low, below 3 %. This is consistent with the earlier observations,

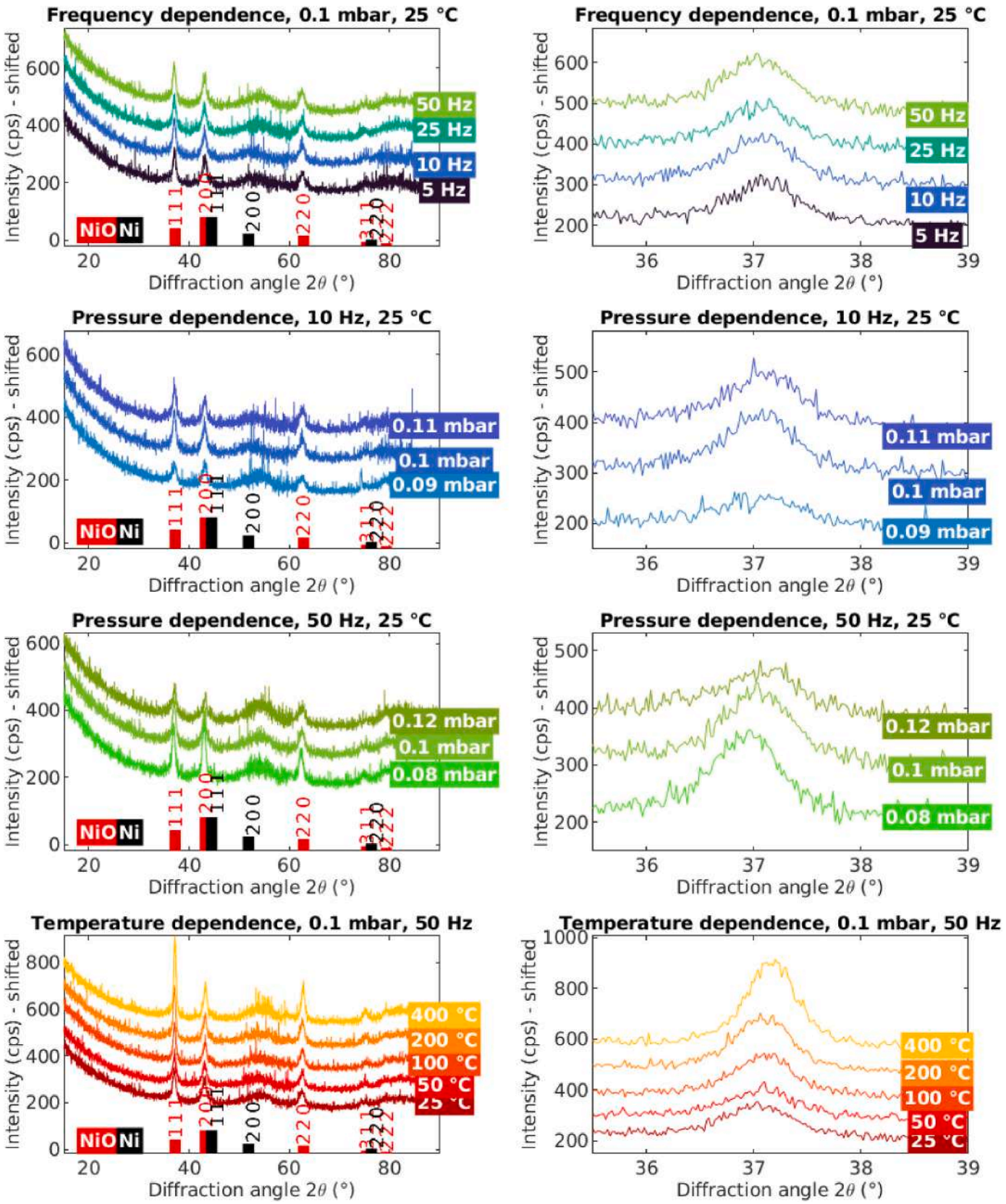

Fig. 9. X-ray diffraction patterns of the NiO_x films deposited by PLD at different conditions showing clearly the polycrystalline nature of the films.

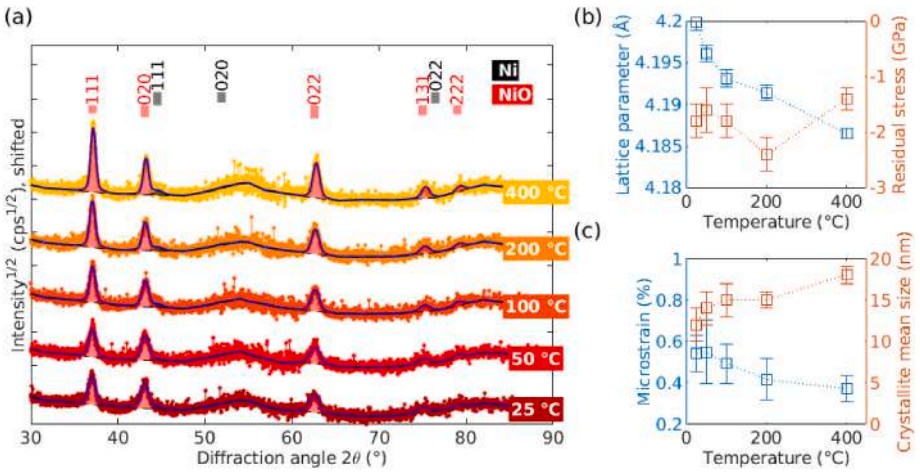

Fig. 10. Fitted X-ray diffraction patterns of NiO_x layers deposited at different substrate temperatures (a) and corresponding lattice parameters (b) and microstrain (c), respectively.

Table 3
Microstructure parameters of NiO_x layers deposited at different temperatures calculated through XRD analysis: minimal NiO and maximal Ni relative weight fraction, NiO lattice parameters, microstrain, crystalline-mean size and residual stress.

T (°C)	Relative weight fraction (%) NiO	Ni	NiO lattice parameter (Å)	Microstrain (%)	Crystallite mean-size(nm)	Residual Stress(GPa)
25	98.8	1.2	4.200 ± 0.001	0.54 ± 0.09	12 ± 2	−1.8 ± 0.3
50	99.7	0.3	4.196 ± 0.001	0.55 ± 0.15	14 ± 2	−1.6 ± 0.4
100	97.5	2.5	4.193 ± 0.001	0.49 ± 0.10	15 ± 2	−1.8 ± 0.3
200	97.7	2.3	4.1914 ± 0.0009	0.42 ± 0.1	15 ± 1	−2.4 ± 0.3
400	97.4	2.6	4.1865 ± 0.0006	0.37 ± 0.06	18 ± 1	−1.4 ± 0.2

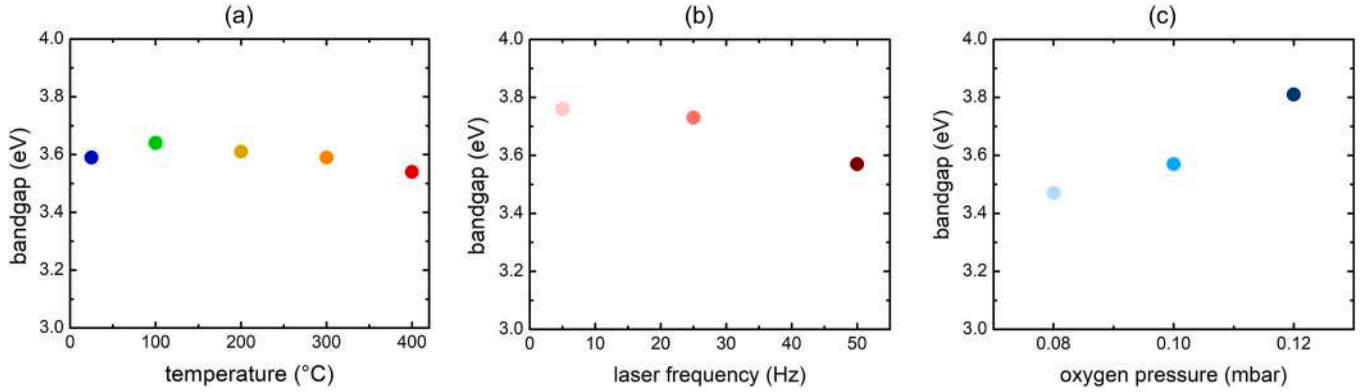

Fig. 11. Bandgap of NiO_x films calculated from the absorption coefficient using a Tauc plot under varying pulsed laser deposition (PLD) conditions (a) temperature, (b) laser frequency and (c) oxygen pressure.

where insufficient oxygen availability likely led to increased defect states in the NiO_x films, hindering charge transport and extraction. As the oxygen pressure increased to 0.1 and 0.15 mbar, we observed a dramatic improvement in average efficiency, peaking around 6 %. This enhancement aligns with the earlier findings that higher oxygen pressures contribute to widening the band gap and reducing sub-gap absorption, leading to fewer defects and better charge transport properties [24]. This improvement in efficiency at moderate pressures suggests an optimal balance between minimising defect states and maintaining the desired optical characteristics of the NiO_x films.

However, at higher pressures of 0.20 mbar and above, we noted a decline in average efficiency or increased variation. This decline could be attributed to the formation of excessive oxide phases or structural changes in the NiO_x material that could adversely affect its transport properties. Such outcomes indicate that while increased oxygen pressure initially enhances efficiency by reducing defects, excessive oxygen can lead to material instability or undesirable phase changes. Fig. 13(b) and (c) show the best-performing PSCs as a function of oxygen pressure and J-V curves of the best-performing PSC, respectively. The highest-performing PSC is observed at 0.15 mbar with a peak efficiency of around 7.8 %, while the device efficiency decreases at both lower and higher pressures.

Fig. 14 shows the effect of pulse number (thickness) on the performance of mixed halide $FA_{0.83}Cs_{0.17}Pb(I_{0.6}Br_{0.4})_3$ PSCs using nickel oxide (NiO_x) as the hole transport layer. At a relatively low number of pulses, specifically 1000, corresponding to the thinnest NiO_x layer, the average efficiency is relatively low, approximately below 4 %, as shown in Fig. 14(a). This can be attributed to inadequate film thickness and potential non-uniformity, which likely resulted in higher defect densities and compromised charge transport properties. As the number of pulses increases to 4000, the average efficiency significantly improves, reaching around 6 %, indicating better film quality and more favourable

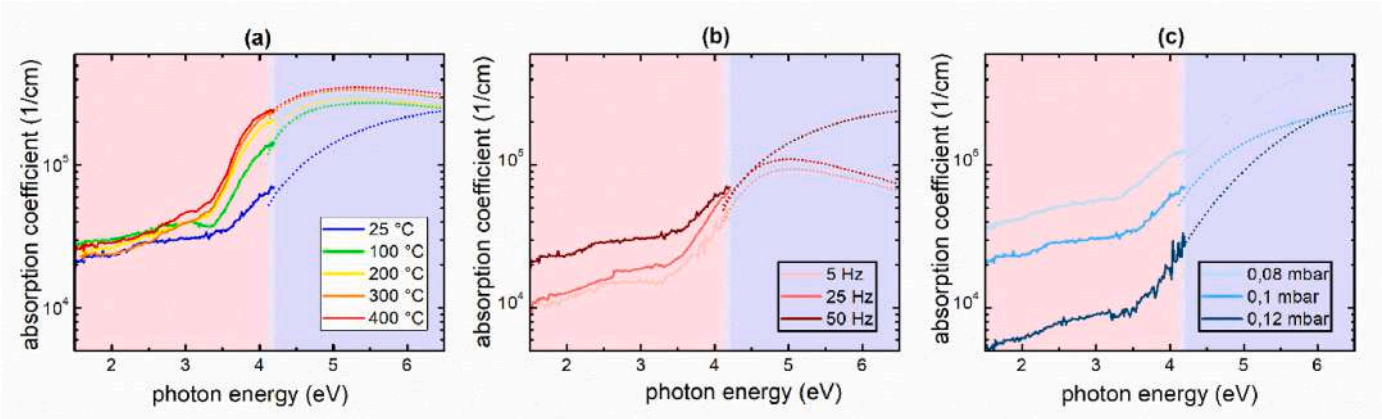

Fig. 12. Absorption coefficient of NiO_x films as a function of photon energy under varying PLD conditions (a) temperature, (b) laser frequency and (c) oxygen pressure. The black dash line shows absorptance of 3 % for layer 10 nm thick.

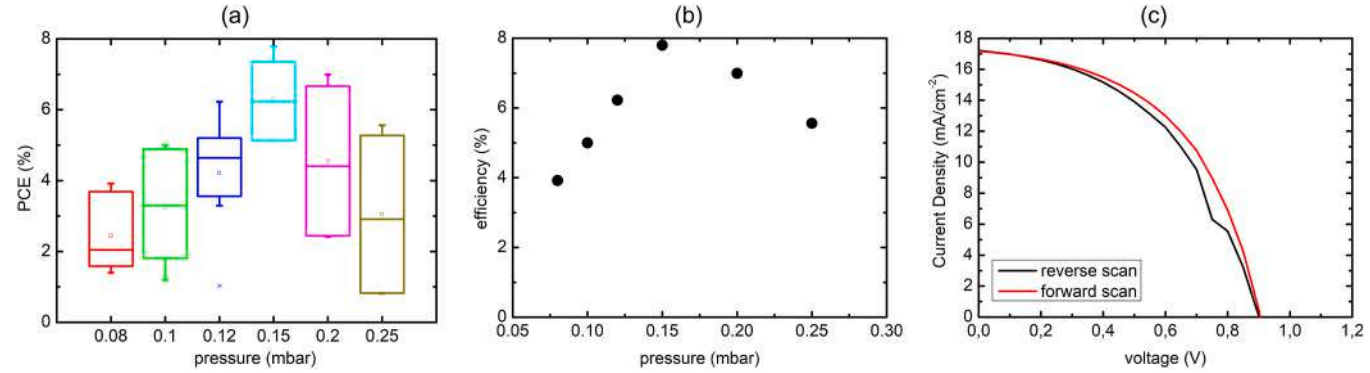

Fig. 13. (a) Power conversion efficiency distribution of the PSCs using NiO_x as the hole transport layer prepared by various oxygen pressures, (b) efficiency of the best-performing PSCs with different oxygen pressures, and (c) current density−voltage (J–V) curves under reverse and forward scans of best performing PSC.

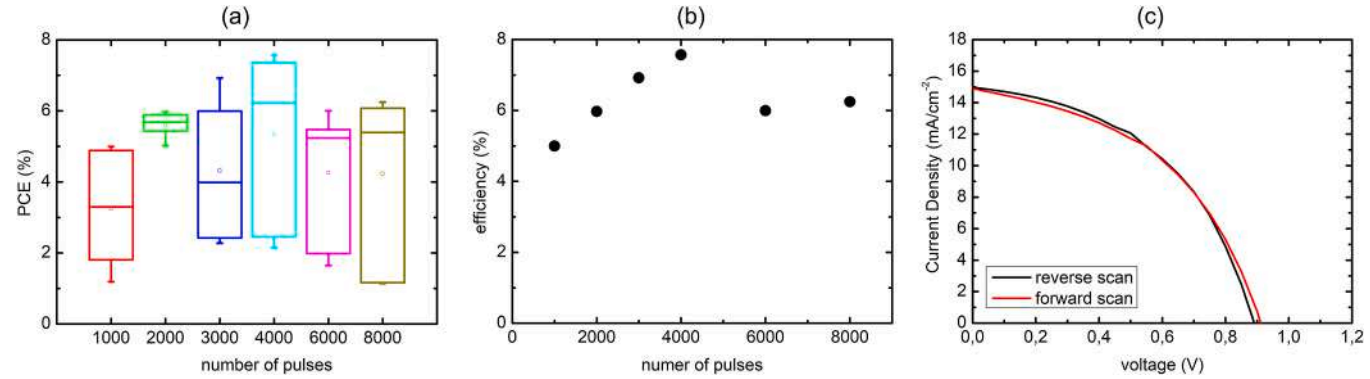

Fig. 14. (a) PCE distribution of the PSCs using NiO_x as the HTL prepared with different numbers of pulses, (b) efficiency of the best-performing PSCs with different numbers of pulses, and (c) current density−voltage (J–V) curves under reverse and forward scans of the best performing PSC.

charge transport characteristics. Beyond 4000 pulses, with thicker NiO_x films, the efficiency starts to decline, showing increased variability at 6000 and 8000 pulses. This is likely due to decreased charge transport efficiency as the thicker layer may introduce more resistance, hampering charge extraction.

Fig. 14(b) shows the efficiency of the best-performing PSCs at each thickness level. Similar to Fig. 9(a), the maximum efficiency is observed at 4000 pulses, where the efficiency reaches 7.6 %. The J−V curve in Fig. 14(c) shows the current density and voltage characteristics of the best-performing PSC under forward and reverse scan directions. The device, prepared with 4000 pulses (optimal thickness), demonstrates minimal hysteresis between the forward (red) and reverse (black) scans.

These findings align well with previous discussions on the effects of oxygen pressure and bandgap tuning. This suggests that an optimal balance can be achieved in terms of bandgap and film thickness, enhancing charge transport and reducing defect states. Furthermore, these findings support the earlier simulation results that indicated how carefully optimised deposition conditions lead to higher solar cell efficiencies.

4. Conclusions

In this study, we successfully prepared NiO_x HTLs by pulsed laser deposition under varying conditions and investigated the effect of bandgap variation on the performance of perovskite solar cells. The study reveals that variations in deposition temperature, laser frequency, and oxygen pressure alter the chemical composition, optical properties, and defect states in NiOx films. The fabrication of $FA_{0.83}Cs_{0.17}Pb(I_{0.6}Br_{0.4})_3$ mixed halide PSCs using PLD-grown NiO_x HTLs with varying oxygen pressures and film thickness resulted in a maximum power conversion efficiency of around 8 %, without the use of an extra dipole layer, confirming PLD as a promising technology for tuning the properties of high-performance HTLs. Combined with theoretical device simulations, these findings highlight the importance of NiO_x bandgap tuning by controlled deposition techniques like PLD in optimising the efficiency of perovskite solar cells.

CRediT authorship contribution statement

Eva Horynova: Writing – original draft, Visualization, Validation, Supervision, Project administration, Investigation, Data curation, Conceptualization. **Jakub Holovsky:** Validation, Supervision, Project administration, Conceptualization. **Lucie Landova:** Methodology, Formal analysis. **Naini Jain:** Writing – original draft, Methodology, Investigation, Data curation, Conceptualization. **Abhinav Deep Pakki:** Investigation. **Meng-Hsueh Kuo:** Investigation, Data curation. **Ivana Beshajová Pelikánová:** Investigation, Conceptualization. **Branislav Dzurňák:** Writing – review & editing, Investigation, Data curation, Conceptualization. **Lukáš Horák:** Writing – review & editing, Methodology, Investigation, Data curation. **Ognen Pop-Georgievski:** Writing – review & editing, Writing – original draft, Visualization, Methodology, Investigation, Data curation, Conceptualization. **Amalraj Peter Amalathas:** Writing – review & editing, Writing – original draft, Visualization, Formal analysis, Data curation. **Neda Neykova:** Writing – review & editing, Writing – original draft, Supervision, Methodology, Investigation.

Declaration of competing interest

The authors declare that they have no known competing financial interests or personal relationships that could have appeared to influence the work reported in this paper.

Acknowledgement

We acknowledge the support of the Czech Ministry of Education, Youth and Sports grant no. CZ.02.01.01/00/22_008/0004617 – "Energy conversion and storage", the Czech Science Foundation GA ČR, grant no. 23-06543S and CTU student grant SGS24/135/OHK3/3T/13.

Appendix A. Supplementary data

Supplementary data to this article can be found online at https://doi.org/10.1016/j.vacuum.2025.114812.

Data availability

Data will be made available on request.

References

[1] T. Singh, T. Miyasaka, Stabilizing the efficiency beyond 20% with a mixed cation perovskite solar cell fabricated in ambient air under controlled humidity, Adv. Energy Mater. 8 (3) (Jan. 2018) 1700677, https://doi.org/10.1002/AENM.201700677.

[2] M.H. Kuo, N. Neykova, I. Stachiv, Overview of the recent findings in the perovskite-type structures used for solar cells and hydrogen storage, Energies 17 (18) (Sep. 2024) 4755, https://doi.org/10.3390/EN17184755, 2024, Vol. 17, Page 4755.

[3] C. Yang, et al., Achievements, challenges, and future prospects for industrialization of perovskite solar cells, Light Sci. Appl. 13 (1) (Sep. 2024) 1–48, https://doi.org/10.1038/s41377-024-01461-x, 2024 13:1.

[4] A. Kojima, K. Teshima, Y. Shirai, T. Miyasaka, Organometal halide perovskites as visible-light sensitizers for photovoltaic cells, J. Am. Chem. Soc. 131 (17) (May 2009) 6050–6051, https://doi.org/10.1021/JA809598R/SUPPL_FILE/JA809598R_SI_001.PDF.

[5] M.A. Green, et al., Solar cell efficiency tables (version 64), Prog. Photovoltaics Res. Appl. 32 (7) (Jul. 2024) 425–441, https://doi.org/10.1002/PIP.3831.

[6] Q. Jiang, et al., Surface passivation of perovskite film for efficient solar cells, Nat. Photonics 13 (7) (Apr. 2019) 460–466, https://doi.org/10.1038/s41566-019-0398-2, 2019 13:7.

[7] C. Momblona, et al., Efficient vacuum deposited p-i-n and n-i-p perovskite solar cells employing doped charge transport layers, Energy Environ. Sci. 9 (11) (Nov. 2016) 3456–3463, https://doi.org/10.1039/C6EE02100J.

[8] M.K. Hossain, et al., An extensive study on multiple ETL and HTL layers to design and simulation of high-performance lead-free CsSnCl3-based perovskite solar cells, Sci. Rep. 13 (1) (Feb. 2023) 1–24, https://doi.org/10.1038/s41598-023-28506-2, 2023 13:1.

[9] M.H. Miah, M.U. Khandaker, M.B. Rahman, M. Nur-E-Alam, M.A. Islam, Band gap tuning of perovskite solar cells for enhancing the efficiency and stability: issues and prospects, RSC Adv. 14 (23) (May 2024) 15876–15906, https://doi.org/10.1039/D4RA01640H.

[10] M. Yang, H. Wang, W. Cai, Z. Zang, Mixed-halide inorganic perovskite solar cells: opportunities and challenges, Adv. Opt. Mater. 11 (20) (Oct. 2023) 2301052, https://doi.org/10.1002/ADOM.202301052.

[11] X. Cai, et al., A review for nickel oxide hole transport layer and its application in halide perovskite solar cells, Mater. Today Sustain. 23 (Sep. 2023) 100438, https://doi.org/10.1016/J.MTSUST.2023.100438.

[12] M. Tao, et al., Molecule-triggered strain regulation and interfacial passivation for efficient inverted perovskite solar cells, Joule 0 (0) (Aug. 2024), https://doi.org/10.1016/j.joule.2024.08.003.

[13] S.K. Kim, et al., Comparison of NiO x thin film deposited by spin-coating or thermal evaporation for application as a hole transport layer of perovskite solar cells, RSC Adv. 10 (71) (Dec. 2020) 43847–43852, https://doi.org/10.1039/D0RA08776A.

[14] M. Jlassi, I. Sta, M. Hajji, H. Ezzaouia, Optical and electrical properties of nickel oxide thin films synthesized by sol–gel spin coating, Mater. Sci. Semicond. Process. 21 (1) (May 2014) 7–13, https://doi.org/10.1016/J.MSSP.2014.01.018.

[15] P. Salunkhe, A.V. Muhammed Ali, D. Kekuda, Investigation on tailoring physical properties of Nickel Oxide thin films grown by dc magnetron sputtering, Mater. Res. Express 7 (1) (Jan. 2020) 016427, https://doi.org/10.1088/2053-1591/AB69C5.

[16] E. Aydin, et al., Room-temperature-sputtered nanocrystalline nickel oxide as hole transport layer for p-i-n perovskite solar cells, ACS Appl. Energy Mater. 1 (11) (Nov. 2018) 6227–6233, https://doi.org/10.1021/ACSAEM.8B01263/SUPPL_FILE/AE8B01263_SI_001.PDF.

[17] H.L. Chen, Y.M. Lu, W.S. Hwang, Characterization of sputtered NiO thin films, Surf. Coat. Technol. 198 (1–3) (Aug. 2005) 138–142, https://doi.org/10.1016/J.SURFCOAT.2004.10.032.

[18] E. Horynová, et al., Optical characterization of low temperature amorphous MoOx, WOX, and VOx prepared by pulsed laser deposition, Thin Solid Films 693 (Jan. 2020) 137690, https://doi.org/10.1016/J.TSF.2019.137690.

[19] J. Zhao, A. Ho-Baillie, S.P. Bremner, Pulsed laser deposition nickel oxide on crystalline silicon as hole selective contacts, J. Vac. Sci. Technol. B 38 (1) (Jan. 2020), https://doi.org/10.1116/1.5124840.

[20] K. Ridzoňová, et al., Correlating light-induced deep defects and phase segregation in mixed-halide perovskites, J Mater Chem A Mater 10 (36) (Sep. 2022) 18928–18938, https://doi.org/10.1039/D2TA03538C.

[21] P. Salunkhe, D. Kekuda, Effect of annealing temperature on the physical properties of NiO thin films and ITO/NiO/Al schottky diodes, J. Mater. Sci. Mater. Electron. 33 (26) (Sep. 2022) 21060–21074, https://doi.org/10.1007/S10854-022-08910-6/FIGURES/14.

[22] C. Zhang, G. Liu, X. Geng, K. Wu, M. Debliquy, Metal oxide semiconductors with highly concentrated oxygen vacancies for gas sensing materials: a review, Sens. Actuator. A Phys. 309 (Jul. 2020) 112026, https://doi.org/10.1016/J.SNA.2020.112026.

[23] S. Timoshnev, et al., Annealing temperature effect on the physical properties of NiO thin films grown by DC magnetron sputtering, Adv. Mater. Interfac. 11 (9) (Mar. 2024) 2300815, https://doi.org/10.1002/ADMI.202300815.

[24] A. Peter Amalathas, L. Landová, K. Ridzoňová, L. Horák, P. Bauerová, J. Holovský, Unveiling the effect of potassium treatment on the mesoporous TiO2/perovskite interface in Perovskite solar cells, ACS Appl. Energy Mater. 4 (10) (Oct. 2021) 11488–11495, https://doi.org/10.1021/ACSAEM.1C02229/SUPPL_FILE/AE1C02229_SI_001.PDF.